# A n-type, Stable Electrolyte Gated Organic Transistor Based on a Printed Polymer

*Fabrizio Antonio Viola,\* Filippo Melloni, Alireza Molazemhosseini, Francesco Modena, Mauro Sassi, Luca Beverina, and Mario Caironi\**

Electrolyte-gated organic transistors (EGOTs) are promising and versatile devices for next-generation biosensors, neuromorphic systems, and low-voltage electronics. They are particularly indicated for applications where stable operation in aqueous environment and cost-effective manufacturing are required. Indeed, EGOTs can be fabricated through low-cost, large area, and scalable techniques, such as printing, from a large portfolio of solution processable organic materials, which are often able to stably operate in water or physiological solutions. Despite a large number of solution processable EGOTs have been reported in the literature so far, only a few are based on printed semiconductors, with no examples of digitally printed, i.e., inkjet printed, n-type devices, which would easily enable complementary architectures. In this work, we propose the first example of a n-type electrolyte gated organic transistor based on an inkjet printed polymer. The proposed device shows a high stability when operated in water and requires only 3 hours of conditioning to produce a stable response, a much faster dynamic than in the case of printed polymers currently tested for p-type EGOTs. As a proof-of-concept, the proposed printed n-type EGOT is successfully integrated with a printed single-walled carbon-nanotubes based p-type device in a logic inverter, demonstrating the possibility to build simple water-gated digital electronic circuits.

## 1. Introduction

Electronic devices capable to stably operate in an aqueous medium offer the opportunity to bridge electronics and biology, and are currently explored for applications such as biosensors or electrophysiology sensors,[1–4] neuromorphic computing[5–7] and digital circuits,[8,9] where signal amplification and low-voltage operation are required. Electrolyte-gated organic transistors (EGOTs) are a well-recognized candidate to fulfill such requirements. Indeed, they offer an intrinsic local amplification of input signals together with the opportunity of a stable, low-voltage operation in water.[10] EGOTs are three-terminal devices based on organic semiconductors, where an ionically conducting and electronically insulating solid or liquid electrolyte is employed as a gate insulator.[11] Depending on the permeability or the impermeability of the organic semiconductor to ions in the electrolyte solution, EGOTs can be divided into two classes.[12] In the former case (permeable organic semiconductor), when a potential is applied to the gate electrode, the ions drift through the electrolyte and can penetrate the semiconductor. Therefore, the field-effect, which induces the accumulation of electronic charge to compensate ionic charge, is extended to the whole three-dimensional volume of the semiconductor. The resulting volumetric capacitance depends on the semiconductor thickness and can reach very large values, in the range of few F cm$^{-3}$.[13,14] These kinds of devices are addressed as organic electrochemical transistors (OECTs). In the case of an organic semiconductor impermeable to the ions, upon polarization of the gate electrode, an electrical double layer (EDL) is formed at the interface between electrolyte and semiconductor. The EDL can be roughly modelized as a sub-nanometric thick capacitor, with capacitance values in the order of 1–10 μF cm$^{-2}$,[12] independent of the semiconductor thickness. In this case, the devices are addressed as electrolyte-gated organic field-effect transistors (EGOFETs).

The volumetric capacitance (in OECTs) or the EDL (in EGOFETs) allows the low voltage operation of EGOTs,[10,12,14] with gate potential that can be reduced to even less than 1 V. The low-voltage operation of EGOTs is fundamental when they are employed as transducer devices for electrophysiology and as biosensors (the gate voltage range is below the limit at which unwanted electrochemical processes occur – such as water electrolysis) or as logic circuits (thanks to very low power consumption).[10,12,14]

To date, most of the solution-processable EGOTs reported in the literature are p-type devices based on spin-coated hole-transporting semiconductors, such as P3HT,[15–19] PEDOT:PSS,[20–25]

F. A. Viola, F. Melloni, A. Molazemhosseini, F. Modena, M. Caironi
Center for Nano Science and Technology @PoliMi
Istituto Italiano di Tecnologia
via Giovanni Pascoli 70/3, Milano 20133, Italy
E-mail: fabrizio.viola@iit.it; mario.caironi@iit.it

F. Modena
Dipartimento di Elettronica
Informazione e Bioingegneria; Politecnico di Milano – Milano
Milano 20133, Italy

M. Sassi, L. Beverina
Department of Materials Science
Università di Milano-Bicocca
via Cozzi 55, Milano 20125, Italy

(iD) The ORCID identification number(s) for the author(s) of this article can be found under https://doi.org/10.1002/aelm.202200573.

**ADVANCED
SCIENCE NEWS**

www.advancedsciencenews.com

**ADVANCED
ELECTRONIC
MATERIALS**

www.advelectronicmat.de

p(g2T-TT),[26] PCPDTBT-SO₃K[27] and PTTP-C₆[28] (see the Supporting Information for the complete semiconductors name). Printed p-type EGOTs have been reported so far, typically based on polymers such as P3HT[29] and PEDOT:PSS.[30–33]

Beside p-type devices, only a few examples of n-type EGOTs have been proposed, since they typically suffer from lower performance and a shorter *operating stability* (i.e., the stability of the output current when the device is operating) with respect to p-type EGOTs.[34,35] The operating stability is relevant to assess the capability of a device to maintain its properties during actual operation. It is interesting to note that, in the context of electrolyte-gated devices, a stable output is usually reached only after a certain amount of time of exposure of the semiconductor to electrolyte, called *stabilization time*, which typically depends on the EGOT active layer, and can range from less than one hour,[36] up to tens of hours.[29]

Most of the n-type EGOTs reported in the literature are typically based on spin-coated or spray-coated semiconductors, such as p(gNDI-g2T),[37–40] C60-TEG[41] or BBL[42,43] (see the Supporting Information for the complete semiconductors name). For n-type EGOTs, the maximum reported operating stability is 60 hours,[44] well below that of p-type EGOTs, which is 200 hours (>8 days).[29]

Within such framework, a current challenge is therefore the fabrication of stable n-type EGOTs through large-area, scalable, and additive printing techniques for the deposition of the organic semiconductor, facilitating future scale-up and cost-effective process flows. Indeed, through printing techniques such as inkjet, the materials can be deposited in a controllable way over both rigid or flexible substrates,[45–49] without a physical mask or master (the spatial resolution depends on the specific technology employed) and with a small production of waste.[50] Moreover, enabling reliable printed n-type EGOT could pave the way for the development of robust complementary electrolyte-gated electronic circuits, where a selective and precise patterning of the active materials and the devices stable operation in an aqueous medium are needed. Complementary EGOTs are highly advantageous especially for bioelectronics, for instance as signal amplifiers of weak biopotentials,[43,51] thanks to their high gain with very low-power consumption and low-voltage operation.

In this work, we present the first EGOT in which its n-type behavior is ensured by an inkjet printed naphthalene-diimide-based co-polymer with glycolated solubilizing chains. The device, gated through ultrapure water, is shown to operate in OECT regime, with the development of a volumetric capacitance upon gating. The proposed EGOT is able to produce a stable output current response after a stabilization time of only three hours, thus showing a faster dynamic than in the case of printed p-type EGOTs.[29,52] Moreover, after the stabilization time, the device can stably operate for at least 18 hours, in line with the best operational stability reported for previous non-printed n-type EGOTs.[44]

As a proof of concept of its use in water-gated printed logic circuitry, we propose a complementary inverter based on the coupling of printed n-type and p-type devices: the circuit is able to operate for more than 15 hours in water with a proper inverting behavior and a high gain, proving its functionality as a building block for electrolyte gated digital electronics.

## 2. Results and Discussion

To realize a printed n-type EGOT, we adopted an active material that is a modification of the well-known poly[N,N′-bis(2octyl-dodecyl)-1,4,5,8-napthalenedicarboximide- 2,6-diyl]-alt-5,5′-(2,2′-bithiophene) (PNDIT2) copolymer,[53] with replacement of alkyl side chains with hybrid ones containing oligo(ethylene glycol) groups. As recently reported,[40,54] the inclusion of glycolated chains increases the material swelling, easing ions penetration through the bulk. At the same time, Kim et al.[55] showed how the use of hybrid side-chains comprising an alkyl spacer between the conjugated backbone and oligo(ethylene glycol) groups can greatly improve OFET mobility values as a result of better morphology and long-range order. We, therefore, decided to synthesize the polymer p(NDI-C4-TEGMe-T2) depicted in **Figure 1**a, having a methyltriglycol tethered to the napthalene units through a C4 alkyl spacer, to exploit an expected trade-off between electron mobility, volumetric capacitance, and processability.[54] The final material was synthesized in high yield by means of direct heteroarylation copolymerization of bithiophene and the corresponding dibromo naphthalenediimide monomer (obtained in good yields through a simple three steps process). The detailed synthetic route of the polymer is reported in the Experimental Section and Supporting Information section, together with the solution NMR that shows a defect-free structure and the presence of a mixture of low molecular weight oligomers ($M_n \approx 4.4$ kg mol$^{-1}$). Furthermore, we report the differential pulse voltammetry (DPV) in the Supporting Information section (Figure S9, Supporting Information), with the extracted values of the highest-occupied molecular orbital (HOMO) and the lowest-unoccupied molecular orbital (LUMO) of the p(NDI-C4-TEGMe-T2).

At first, we assess the ion-permeating behavior of the proposed semiconductor, when exposed to ultrapure water and biased, by means of electrochemical impedance spectroscopy (EIS). The structures under test were composed by a metal–semiconductor-water-metal stack (the architecture is shown in Figure 1b). They were fabricated in a two-terminals configuration, with a gold bottom electrode in contact with the semiconductor layer, patterned by inkjet, and a silver coil as the top electrode immersed in the water. We here adopted ultrapure (Milli-Q, Millipore) water, characterized by a resistivity of 10 MΩ cm at 25 °C. Upon contamination by carbon dioxide from the air, water resistivity decreases to hundreds of kΩ cm,[56] and the presence of $H^+$ and $H_3O^+$ ions contributes to the gating of the device. Inkjet printing was selected as the organic semiconductor deposition technique, since it offers simple way to laterally pattern the printed layer, with a good resolution and low waste of active material. We tested stacks with the semiconductor films printed with three different thicknesses, which were tuned by varying the drop spacing (DS) parameter, i.e., the spacing between adjacent droplets in the inkjet printer deposition. The mean and standard deviation values for each thickness are reported in **Table 1**. The limited standard deviations – 16%, 18%, and 21% of the mean value, for the semiconductors printed with a DS of 15, 30, and 45 μm, respectively – indicate a good reproducibility of the thickness.

The EIS analysis was performed in the 50 mHz–1 MHz range, applying a sinusoidal wave ($V_{peak} = 25$ mV) in addition to
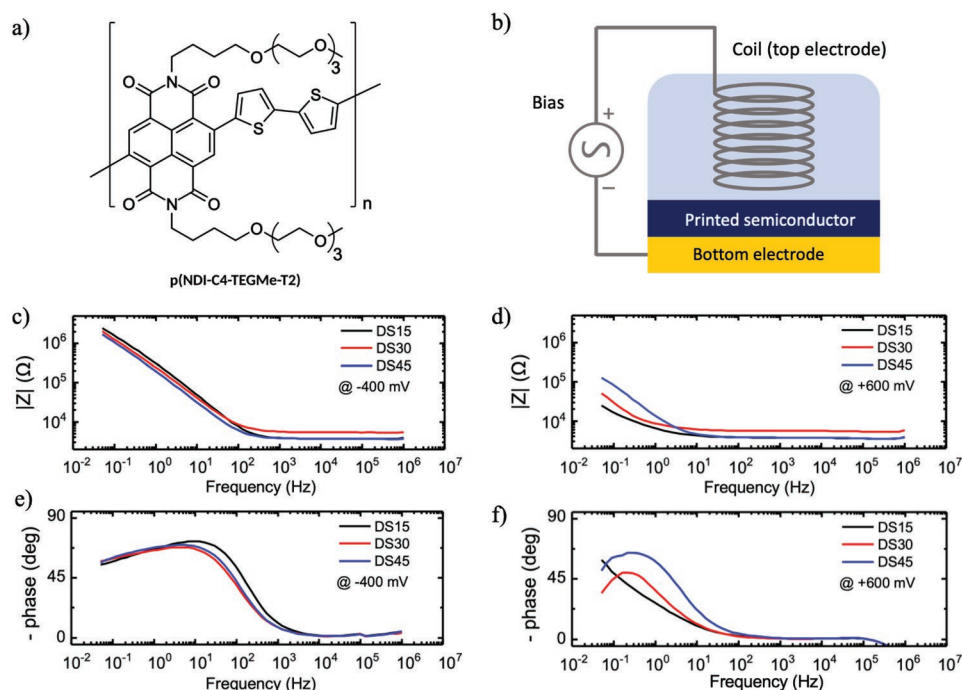
**Figure 1.** a) p(NDI-C4-TEGMe-T2) molecular structure. b) Structure employed for the EIS measurements in a two-terminal configuration. c,d) Module of the Bode diagram of the metal-water-semiconductor stack integrating different semiconductor thicknesses (DS15 = 61 nm; DS30 = 27 nm; DS45 = 16 nm) at different bias. e,f) Phase of the Bode diagram of the metal-water-semiconductor stack integrating different semiconductor thicknesses at different bias.

a DC bias ranging between −400 and +600 mV. In Figure S2a–f, Supporting Information the complete EIS characterization of the realized structures is reported, while Figure S3, Supporting Information shows the fitting of the experimental curves at different bias with an equivalent model circuit. In the equivalent circuit, the low frequency (below 100 Hz) behavior is described by a constant phase element that grasps the complex phenomena at the water-semiconductor interface. Roughly above 100 Hz, a series resistance component dominates the spectra. The complete description of the model is reported in the Supporting Information.

EIS measurements reveal the relation between the semiconductor thickness and the device impedance (Figure 1c–f). When a negative bias is applied at the top electrode, an impedance in the order of MΩ is observed at 100 mHz, weakly affected by the semiconductor thickness. While, when a positive bias is applied, as a result of n-type field-effect and charge accumulation, the impedance at low frequency is decreased by more than an order of magnitude, with a strong influence of the semiconductor thickness. Importantly, the impedance module of the stack scales with the semiconductor thickness, from

82 kΩ (for the 16 nm ± 4 nm thick semiconductor) to 16 kΩ (for the 61 nm ± 10 nm thick semiconductor) at 100 mHz. These observations are compatible with cations penetration in the semiconductor layer,[14,57] and are in line with what has been reported for similar semiconducting layers with ethylene glycol side chains.[40,54]

We then assessed the proper operation of EGOTs based on printed p(NDI-C4-TEGMe-T2), adopting ultrapure water as the electrolyte gating medium. We fabricated 45 devices by printing thin films of semiconductors with the same three thicknesses used for the EIS measurements. In particular, 15 devices were fabricated by printing the organic semiconductor with Drop Spacing 15 μm (thickness 61 ± 10 nm), 15 devices with Drop Spacing 30 μm (thickness 27 ± 5 nm), and 15 devices with Drop Spacing 45 μm (thickness 16 ± 4 nm). The architecture of the presented EGOT device is reported in **Figure 2**a, while its fabrication is reported in the Experimental Section.

From the transfer curves reported in Figure 2b a proper n-type operation at very low gate voltages (from −400 mV to +600 mV) can be appreciated. We obtained a clear correlation of the hysteresis with the scan rate (SR), as reported in Figure 2b,c, Figures S4 and S5, Supporting Information. Such correlation is a well-known behavior of EGOTs based on ion-permeable semiconductors,[14] and confirm the observations and results obtained during the EIS characterization at positive biasing (cations penetration in the semiconductor layer).

The EGOTs average transfer characteristics acquired with a SR equal to 4 mV/sec (reported in **Figure 3**a for the EGOTs with the semiconductor thickness of 61 nm, and in Figure S6, Supporting Information for the EGOTs with the semiconductor

**Table 1.** Statistics (mean and standard deviation calculated on 10 samples) of the thickness values of the printed organic semiconductor.

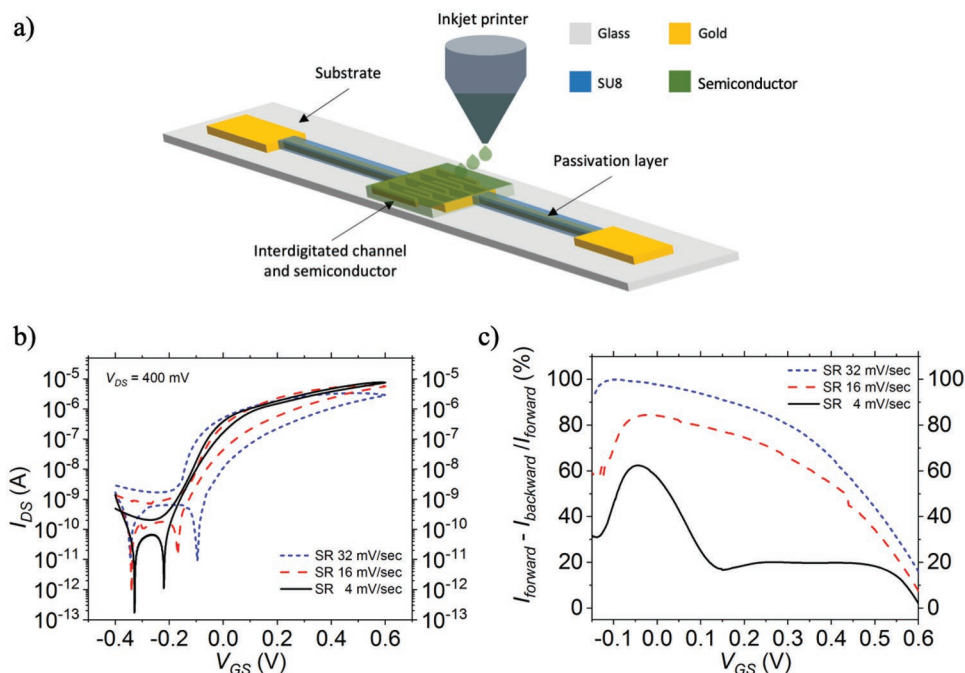| Drop Spacing (μm) | Mean thickness (nm) | Standard deviation (nm) |
|---|---|---|
| 15 | 61 | 10 |
| 30 | 27 | 5 |
| 45 | 16 | 4 |

**Figure 2.** a) Lateral view scheme and overview of the printed n-type EGOT; b) transfer curves acquired at different scan rates for a device with 61 nm thick printed semiconductor; c) normalized hysteresis for a device with 61 nm thick printed semiconductor, calculated as the difference between $I_{DS}$ in forward and backward scans, for different scan rates at the same gate and drain voltage.

thickness of 27 and 16 nm) showed very high repeatability and reproducibility especially for the thicker semiconductor, with a very limited $I_{DS}$ standard deviation of 0.5 µA – which corresponds to the 6% of the mean value – on a mean value of 8.9 µA (evaluated on 13 devices) at $V_{GS}$ = 600 mV. Such reproducibility is not easily observed when a large-area compatible deposition process is adopted,[58] while being a prerequisite for enabling circuit fabrication. As expected from the EIS
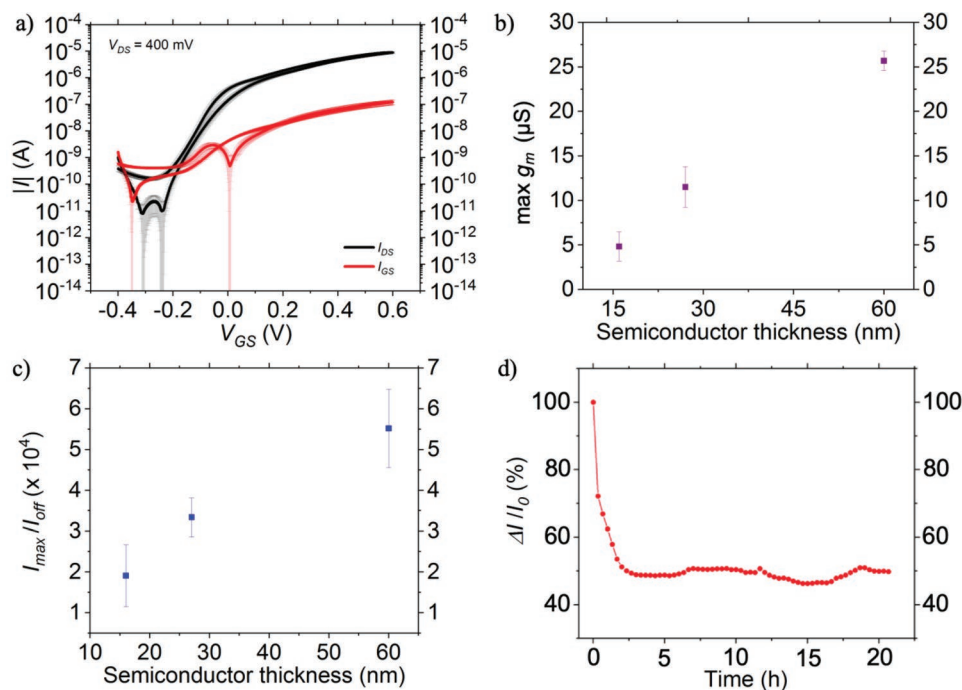


**Figure 3.** a) Average transfer characteristic curves in saturation, with their standard deviation, obtained on 13 EGOTs with 61 nm thick printed semiconductor; b) maximum transconductance values and c) on/off current values for EGOTs with different organic semiconductor thicknesses; d) stability test of n-type EGOT with 61 nm thick printed semiconductor.

**ADVANCED**
SCIENCE NEWS
www.advancedsciencenews.com

**ADVANCED**
ELECTRONIC
**MATERIALS**
www.advelectronicmat.de

characterization, the maximum transconductance $g_m$ (calculated for $V_{GS} = 600$ mV) scales with the thickness of the organic semiconductor,[14] reaching a highly repeatable value of $26 \pm 1$ µS (the standard deviation corresponds to less than 4% of the mean value, evaluated on 13 devices) for the EGOTs with the semiconductor thickness of 61 nm (Figure 3b). In order to favor the comparison of our devices with the nonprinted n-type EGOTs reported in the literature so far, we have characterized our best devices (i.e., those with 61 nm-thick organic semiconductor) by using 0.1 M NaCl as electrolyte and a Ag/AgCl gate electrode, since they are the typical medium and gate used in literature (see Figure S11, Supporting Information section). The new extracted value of the maximum transconductance $g_m$ (calculated for $V_{GS} = 600$ mV) in this condition is $370 \pm 40$ µS, due to a higher presence of ions in solution than pure water, as expected. As reported in Figure S9 and in Table S3, Supporting Information, our proposed printed p(NDI-C4-TEGMe-T2) based EGOTs show higher normalized (to all channel dimensions, i.e., width, length, and thickness) transconductance than the P-90[39] and C60-TEG[41] based devices, and slightly lower, but still comparable, performance with spin coated P-90:TBAF (40 mol%)[39] and p(gNDI-gT2)[40] based OECTs.

Overall, the current on/off ratio (where the on value is the maximum current value calculated at $V_{GS} = 600$ mV, while the off value is the minimum value of the current during the backward scan – typically at $V_{GS}$ between $-300$ and $-200$ mV) is well above $10^4$ for all the devices, as shown in Figure 3c, exceeding the values obtained so far with nonprinted n-type EGOTs.[37–39,41,42] Furthermore, the success rate of the fabrication process reached a value of more than 95% of working devices (only 2 devices – on a total of 45 – did not work, owing to a defect in the photolithographically defined gold bottom contacts), indicating the robustness of the lab-scale fabrication process.

The stability of the printed n-type EGOT when gated through water was then evaluated. At first, we assessed and monitored the EGOT stabilization time following a well-known protocol for a duration of 21 hours, which consists on the measurements of consecutive transfer curves with forward and backward gate voltage scanning.[10,29,36] In order to quantify any variation in device response in the on state, during the stabilization test, the normalized change in channel current at a fixed potential ($\Delta I/I_0$ at $V_{GS} = 600$ mV, where $I_0$ is the current at the beginning of the stability test) was extracted and plotted versus time. According to Figure 3d, the most significant variations of the current were recorded in the first 3 hours, which, therefore, can be considered as the stabilization time of the device. The proposed printed n-type device shows a shorter stabilization time than the values reported for inkjet printed polymer-based p-type EGOTs (>30 hours),[29,52] thus significantly reducing the time constraints on its actual use, as a transducer in a highly sensitive biosensor,[29] for instance. The shorter stabilization time could be likely due to the inclusion of the oligo(ethylene glycol) groups as side chains in the PNDIT2 copolymer, which can increase the material swelling, easing fast ions penetration through the bulk.

After the stabilization time, the device maintains a stable current for the remaining 18 hours, with small residual shifts of the current that do not exceed 3% per hour (Figure S10, Supporting Information section reports the transfer curves from the third to the 21st hour). The operation stability of the device is therefore in excess of 18 hours, and is at par with the best value reported for previous nonprinted n-type EGOTs.[44]

As a proof-of-concept, we built a complementary inverter, to demonstrate the capability of the proposed n-type device to be integrated with a p-type counterpart for applications such as water-operated low-power digital logic circuitry or signal amplifiers for bioelectronics. The electrolyte-gated inverter is fabricated by printing two semiconductors, p(NDI-C4-TEGMe-T2) and monochiral single-walled carbon nanotubes (s-SWCNT), over interdigitated gold contacts (see Figure S13, Supporting Information for the inverter circuit scheme and for transfer curves of the p-type electrolyte-gated transistor). The choice of polymer-wrapped s-SWCNTs is related to their well-known solution processability, compatibility with printing techniques, and their successful adoption as an active layer in electrolyte-gated transistors, achieving high performance and high stability in water.[52,59,60] In an inverter circuit, the transistors share the same gate electrode (which acts as input node) and their drain terminals are electrically connected (acting as output node). Since both the n-type and p-type devices have been fabricated on the same substrate, and the semiconductors are deposited through the same printing technique, their integration into complementary logic circuits is highly simplified. The voltage transfer curves (VTC) have been measured, sweeping the voltage input signal from a "0" logic state (0 V) to a "1" (0.8 V), while the supply voltage was set to 0.8 V. The first VTC measured ($t = 0$ hour) and reported in **Figure 4**a, shows a proper inverting behavior, with an inverting threshold voltage of 0.47 V for the forward scan and 0.43 V for the backward scan, calculated from the intersection point between the VTC and the bisector of the axes. The VTC shows a maximum hysteresis of 37%, owing to the small hysteretic behavior of the n-type EGOT, which does not affect the proper operation of the inverter. The gain values, obtained as the derivative of the VTC, amount to $\approx 8$ V/V as shown in Figure 4b. Moreover, as it can be appreciated from Figure 4 a,b, the inverting behavior and the gain of the inverter are retained after 17 hours in water (exceeding the operating stability of a recent complementary OECTs-based inverter[43]), with an inverting threshold voltage of 0.4 V for the forward scan and 0.35 V for the backward scan, slightly shifted compared with the values at $t = 0$ hour, and a VTC maximum hysteresis of 25%.

## 3. Conclusions

In conclusion, we have proposed the first n-type electrolyte gated organic transistor based on an inkjet printed polymer. The device shows an operational stability of more than 18 hours, with on/off ratio above $10^4$. The electrical characterization demonstrated a good reproducibility of the devices performance, especially in terms of maximum output current and transconductance – equal to $8.9 \pm 0.5$ µA and $26 \pm 1$ µS, respectively – for the devices with the semiconductor thickness of 61 nm, while the maximum transconductance reaches a value of $370 \pm 40$ µS, when the devices are measured with a Ag/AgCl gate electrode and 0.1 M NaCl as gate electrolyte. Furthermore, as a proof-of-concept, we successfully integrated the proposed printed n-type EGOT with a printed p-type device in an inverter gate able to operate in water
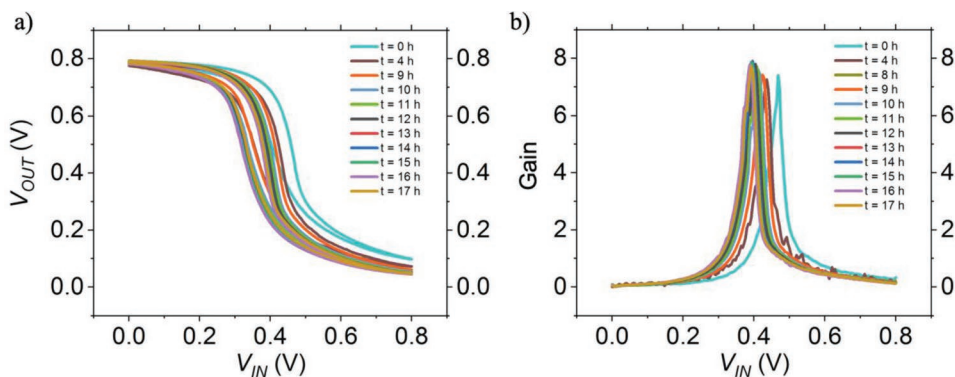
**Figure 4.** a) Voltage transfer curves and b) gain curves of the printed electrolyte gated inverter and stability measurements.

for more than 15 hours with a proper inverting behavior and a substantially stable gain. Overall, besides providing a valid and cost-effective technological solution for the fabrication of EGOTs, which make possible the integration of n-type and p-type devices, the proposed approach can be a candidate for a plethora of possible use ranging from biosensing, for healthcare or biomedical applications, to complementary circuitry, where reproducibility, high operating stability, and low-voltage operation are required.

## 4. Experimental Section

Reagents and solvents were bought from Fluorochem or Sigma–Aldrich. 4,9-Dibromoisochromeno[6,5,4-*def*]isochromene-1,3,6,8-tetraone (NDA-Br$_2$) was bought from TCI chemicals. Filtration on Celite was performed using Celite 535. Column chromatography was performed using DAVISIL LC60A 30–200 μm as a stationary phase. Compositions of solvent mixtures used as eluents were indicated as volume/volume ratios. NMR spectra were collected on a Bruker NMR Avance 400 NEO.

The synthesis of 15-bromo-2,5,8,11-tetraoxapentadecane, 2,5,8,11-tetraoxapentadecan-15-amine and 4,9-dibromo-2,7-di(5,8,11,14-tetraoxapentadec-1-yl)-benzo[*lmn*][3,8]phenanthroline-1, 3, 6, 8(2*H*, 7*H*)-tetraone (NDI-Br$_2$-C4-TEGMe) were reported in Supporting Information.

*p(NDI-C4-TEGMe-T2) Synthesis*: In a screw capped ACE Glass 15 mL pressure tube a mixture of K$_2$CO$_3$ (241 mg, 1.74 mmol), pivalic acid (59.3 mg, 0.581 mmol), NDI-Br$_2$-C4-TEGMe (500 mg, 0.581 mmol) and freshly distilled 2,2'-bithiophene (96.6 mg, 0.581 mmol) was prepared. A solution of Pd$_2$(dba)$_3$ (5.3 mg, 5.81 μmol) in anhydrous chlorobenzene (2.3 mL) was added. The tube was sealed and the resulting mixture was stirred at room temperature for 10 min and then heated to 110 °C. After 20 h the mixture was cooled to room temperature and dissolved in 10 mL of CHCl$_3$. The product was reprecipitated by the addition of the solution to 75 mL of EtOH under constant stirring. The obtained blue suspension was filtered through a cellulose extraction thimble. The product was continuously extracted in a Soxhlet apparatus with MeOH, acetone, petroleum ether, and THF in the stated order. Finally, extraction with CHCl$_3$ was performed. The CHCl$_3$ extract was evaporated to 15 ml and dropwise added to 75 mL of MeOH. The precipitated purified product was recovered as a dark blue powder by centrifugation and subsequent evaporation of residual solvent under reduced pressure (386 mg, 0.446 mmol, yield 77%).

*Molecular Weight (Mn) Determination by $^1$H NMR*: As already reported in Ohayon et al.[54] the aggregation behavior of the polymer, induced by the presence glycol chains, makes molecular weight determination by established SEC methods impossible. Alternative methods were therefore required to assess Mn for the polymer. Taking advantage of the existing and detailed NMR studies on direct heteroarylation polymerization of 2,2'-bithiophene and 4,9-Dibromo-2,7-bis(2-octyldodecyl)benzo[*lmn*][3,8]phenanthroline-1,3,6,8(2*H*,7*H*)-tetraone to obtain the closely related

PNDIT2,[61] we therefore identified characteristic signal of terminal groups from the polymer $^1$H NMR spectrum in C$_2$D$_2$Cl$_4$ at 100 °C (reported in Supporting Information).

Namely the obtained NMR spectra highlight the absence of homo coupling defect and the presence of just two types of chain terminations: NDI-bithiophene (5 signals in the 7.12 – 7.42 region. The integral from the clean and nonoverlapping quartet centered at 7.15 was used for calculations) and NDI-OH (two characteristic singlets at 8.81 and 8.44 ppm), see the Supporting Information for the details. The latter arise from nucleophilic aromatic substitution of pivalate on the naphthalene diimide core that later undergoes hydrolysis during workup. The extent of such type of termination in the present case could be attributed to the polar local environment resulting from the presence of the glycol chains that enhance the nucleophilicity of pivalate. A similar observation was already reported by Matsidik et al.[62] when performing direct heteroarylation polymerization in polar media. The presence of such termination mechanism also justifies the rather low molecular weight obtained.

Starting from NMR signals integration the molar ratio ($\alpha$) between in-chain NDI units and NDI terminal units (NDI-OH + NDI-bithiophene) along with the ratio between the two types of terminations (OH/Bth, $\beta$) were calculated ($\alpha = 1.53$, $\beta = 0.76$). From these data Mn can be calculated as follows:

$$\begin{aligned}
\text{Mn} &= \text{MM}_{\text{NDI}} \cdot n_{\text{NDI}} + \text{MM}_{\text{BTh}} \cdot n_{\text{BTh}} + \text{MM}_{\text{BThH}} \cdot n_{\text{termBTh}} \\
&\quad + \text{MM}_{\text{OH}} \cdot n_{\text{termOH}} = \text{MM}_{\text{NDI}} \cdot (\alpha \cdot 2 + 2) + \text{MM}_{\text{BTh}} \cdot (\alpha \cdot 2 + 1) \\
&\quad + \text{MM}_{\text{BThH}} \cdot (2/(1+\beta)) + \text{MM}_{\text{OH}} \cdot 2 \cdot (1 - 1/(1+\beta)) \\
&= 700.8 \text{ g/mol} \cdot (\alpha \cdot 2 + 2) + 164.2 \text{ g/mol} \cdot (\alpha \cdot 2 + 1) \\
&\quad + 165.2 \text{ g/mol} \cdot (2/(1+\beta)) + 17.01 \text{ g/mol} \cdot 2 \cdot (1 - 1/(1+\beta)) = 4.4 \text{ kg/mol}
\end{aligned} \tag{1}$$

with an average number of 5.0 NDI units per chain.

The synthesis scheme of p(NDI-C4-TEGMe-T2) is reported in Figure S10, Supporting Information.

*EGOTs Fabrication*: Interdigitated source-drain electrodes with $W = 10$ mm and $L = 10$ μm were patterned on a glass substrate by a mask-less image reversal lithography process (AZ5214E photoresist together with a MLA100 Heidelberg mask-less aligner), including thermal evaporation of chromium (2 nm) and gold (40 nm), followed by lift-off in N-methyl-2-pyrrolidone. Gold electrodes were subjected to 3 min of oxygen plasma treatment before inkjet printing. The p(NDI-C4-TEGMe-T2) ink was inkjet-printed (Fujifilm Dimatix, DMP2831) from a 1,2-dichlorobenzene-based solution, and a concentration of 3 mg ml$^{-1}$, through a cartridge with 10 pL nozzles onto the active area of the patterned electrodes (an area of 900 × 660 μm$^2$) with Drop Spacing of 15, 30 and 45 μm. The firing voltage was set to 35 V, the jetting frequency was set to 1 kHz and the printer plate temperature was set to 35 °C. A film of inkjet-printed insulator (SU8 – TF6001 MicroChem) was employed to selectively passivate source and drain electrodes. It was printed through a cartridge with 10 pL nozzles, at a Drop Spacing of 20 μm, a firing voltage of 35 V, and a jetting frequency of 5 kHz and

the printer plate temperature was set to 35 °C. Printed patterns were annealed for 120 min at 120 °C in a nitrogen environment.

*EGOTs Electrical Characterization and Stability*: The electrical characterization of the EGOTs was performed by means of an Agilent Technologies B1500A Semiconductor Device Parameter Analyzer. A tungsten gate electrode was immersed within the ultrapure water (Milli-Q, Millipore) and employed for testing the device. They were interrogated by consecutive recordings of transfer characteristic curves with different scan rates (4, 16 or 32 mV s$^{-1}$). The stability measurement was performed for 21 hours with an interval of 12 min, by acquiring consecutive transfer curves every 12 min (each curve acquisition lasts for 8 min). The protocol considers $\Delta I$ stable when the rate of the ratio between its temporal variation ($\Delta I$) and its initial value ($I_0$) reaches 0.003 h$^{-1}$.

*Inverter Characterization and Stability*: For the proof-of-concept experiment, i.e., the complementary inverter logic gate built with the n-type and p-type devices, the same setup used for electrical characterization of the single n-type EGOT was used, adopting a tungsten gate electrode. The inverter was interrogated by consecutive recordings of voltage transfer curves (VTC).

*Electrochemical Impedance Spectroscopy*: Electrochemical impedance spectroscopy was performed with a potentiostat – Metrohm Autolab PGSTAT 302 – in a two-terminal configuration (i.e., the reference and counter electrodes were shorted on one of the electrodes, while the working electrode and sense were shorted on the opposite side). The semiconductor/water contact area is 38.5 mm$^2$, much smaller than the area of the coil (which acts as a working electrode) immersed in the ultrapure water (Milli-Q, Millipore) ($\approx$950 mm$^2$). The spectra were recorded in the 50 mHz–1 MHz range, applying to the device a sinusoidal wave signal with a 25 mV peak, superimposing a constant bias between −400 and 600 mV.

*Differential Pulse Voltammetry (DPV)*: DPV electrochemical measures were carried out using a potentiostat – PARSTAT 2273 – in a single chamber, three electrodes electrochemical cell, in a glove box filled with Argon ([O2] $\leq$ 1 ppm). Glassy carbon (GC) pin was used as working electrode. The counter and pseudo reference electrodes were a Pt flag and a Ag/AgCl wire, respectively. GC pin was well polished with alumina 0.1 µm suspension, sonicated for 15 min in acetone, and washed with 2-propanol before use. The Ag/AgCl pseudo reference electrode was calibrated before and after each measurement using a 1 × 10−3 M ferrocene solution in the electrolyte; no more than 5 mV difference was observed between two successive calibrations. In calculating the HOMO and LUMO energies, an absolute energy of −5.1 eV versus vacuum level was assigned to the ferrocene/ferrocenium (Fc/Fc$^+$) couple. The electrochemical measurements on the polymer sample were carried out by drop casting CHCl$_3$ solution of the polymer on the polished GC electrode surface. A tetrabutylammonium perchlorate 0.1 M (TBAClO$_4$ 0.1 M) solution in acetonitrile was used as an electrolyte.

## Supporting Information

Supporting Information is available from the Wiley Online Library or from the author.

## Acknowledgements

## Conflict of Interest

The authors declare no conflict of interest.

## Data Availability Statement

The data that support the findings of this study are available from the corresponding author upon reasonable request.

## Keywords

[1] K. B. Parizi, X. Xu, A. Pal, X. Hu, H. S. Philip Wong, *Sci. Rep.* **2017**, *7*, 41305.

[2] S. Nakata, T. Arie, S. Akita, K. Takei, *ACS Sens.* **2017**, *2*, 443.

[3] G. Xu, J. Abbott, D. Ham, *IEEE Trans. Electron Devices* **2016**, *63*, 3249.

[4] A. Spanu, N. Colistra, P. Farisello, A. Friz, N. Arellano, C. T. Rettner, A. Bonfiglio, L. Bozano, S. Martinoia, *J. Neural Eng.* **2020**, *17*, 036033.

[5] J. Zhou, Y. Liu, Y. Shi, Q. Wan, *IEEE Electron Device Lett.* **2014**, *35*, 280.

[6] J. Sun, S. Oh, Y. Choi, S. Seo, M. J. Oh, M. Lee, W. B. Lee, P. J. Yoo, J. H. Cho, J. H. Park, *Adv. Funct. Mater.* **2018**, *28*, 1804397.

[7] L. Guo, J. Wen, J. Ding, C. Wan, G. Cheng, *Sci. Rep.* **2016**, *6*, 38578.

[8] D. Weller, G. Cadilha Marques, J. Aghassi-Hagmann, M. B. Tahoori, *IEEE Electron Device Lett.* **2018**, *39*, 831.

[9] G. Cadilha Marques, S. K. Garlapati, S. Dehm, S. Dasgupta, H. Hahn, M. Tahoori, J. Aghassi-Hagmann, *Appl. Phys. Lett.* **2017**, *111*, 102103.

[10] F. Torricelli, D. Z. Adrahtas, Z. Bao, M. Berggren, F. Biscarini, A. Bonfiglio, C. A. Bortolotti, C. D. Frisbie, E. Macchia, G. G. Malliaras, I. McCulloch, M. Moser, T.-Q. Nguyen, R. M. Owens, A. Salleo, A. Spanu, L. Torsi, *Nat. Rev. Methods Prim.* **2021**, *1*, 66.

[11] L. Kergoat, L. Herlogsson, D. Braga, B. Piro, M. C. Pham, X. Crispin, M. Berggren, G. Horowitz, *Adv. Mater.* **2010**, *22*, 2565.

[12] S. H. Kim, K. Hong, W. Xie, K. H. Lee, S. Zhang, T. P. Lodge, C. D. Frisbie, *Adv. Mater.* **2013**, *25*, 1822.

[13] J. Rivnay, P. Leleux, M. Ferro, M. Sessolo, A. Williamson, D. A. Koutsouras, D. Khodagholy, M. Ramuz, X. Strakosas, R. M. Owens, C. Benar, J. M. Badier, C. Bernard, G. G. Malliaras, *Sci. Adv.* **2015**, *1*, e1400251.

[14] J. Rivnay, S. Inal, A. Salleo, R. M. Owens, M. Berggren, G. G. Malliaras, *Nat. Rev. Mater.* **2018**, *3*, 17086.

**ADVANCED
SCIENCE NEWS**

www.advancedsciencenews.com

**ADVANCED
ELECTRONIC
MATERIALS**

www.advelectronicmat.de

[15] E. Macchia, L. Sarcina, R. A. Picca, K. Manoli, C. Di Franco, G. Scamarcio, L. Torsi, *Anal. Bioanal. Chem.* **2020**, *412*, 811.

[16] S. K. Sailapu, E. Macchia, I. Merino-Jimenez, J. P. Esquivel, L. Sarcina, G. Scamarcio, S. D. Minteer, L. Torsi, N. Sabaté, *Biosens. Bioelectron.* **2020**, *156*, 112103.

[17] E. Macchia, K. Manoli, B. Holzer, C. Di Franco, R. A. Picca, N. Cioffi, G. Scamarcio, G. Palazzo, L. Torsi, *Anal. Bioanal. Chem.* **2019**, *411*, 4899.

[18] L. Sarcina, F. Viola, F. Modena, R. A. Picca, P. Bollella, C. Di Franco, N. Cioffi, M. Caironi, R. Österbacka, I. Esposito, G. Scamarcio, L. Torsi, F. Torricelli, E. Macchia, *Anal. Bioanal. Chem.* **2022**, *414*, 5657.

[19] E. Macchia, L. Sarcina, C. Driescher, Z. Gounani, A. Tewari, R. Osterbacka, G. Palazzo, A. Tricase, Z. M. Kovacs Vajna, F. Viola, F. Modena, M. Caironi, F. Torricelli, I. Esposito, L. Torsi, *Adv. Electron. Mater.* **2021**, *7*, 2100304.

[20] K. Guo, S. Wustoni, A. Koklu, E. Díaz-Galicia, M. Moser, A. Hama, A. A. Alqahtani, A. N. Ahmad, F. S. Alhamlan, M. Shuaib, A. Pain, I. McCulloch, S. T. Arold, R. Grünberg, S. Inal, *Nat. Biomed. Eng.* **2021**, *5*, 666.

[21] S. T. Keene, D. Fogarty, R. Cooke, C. D. Casadevall, A. Salleo, O. Parlak, *Adv. Healthcare Mater.* **2019**, *8*, 1901321.

[22] P. Onur, K. S. Tom, M. Andrew, C. V. F. , S. Alberto, *Sci. Adv.* **2022**, *4*, eaar2904.

[23] P. Leleux, J. Rivnay, T. Lonjaret, J. M. Badier, C. Bénar, T. Hervé, P. Chauvel, G. G. Malliaras, *Adv. Healthcare Mater.* **2015**, *4*, 142.

[24] Y. Van De Burgt, E. Lubberman, E. J. Fuller, S. T. Keene, G. C. Faria, S. Agarwal, M. J. Marinella, A. Alec Talin, A. Salleo, *Nat. Mater.* **2017**, *16*, 414.

[25] D. Khodagholy, T. Doublet, P. Quilichini, M. Gurfinkel, P. Leleux, A. Ghestem, E. Ismailova, T. Hervé, S. Sanaur, C. Bernard, G. G. Malliaras, *Nat. Commun.* **2013**, *4*, 1575.

[26] V. Venkatraman, J. T. Friedlein, A. Giovannitti, I. P. Maria, I. McCulloch, R. R. McLeod, J. Rivnay, *Adv. Sci.* **2018**, *5*, 1800453.

[27] A. T. Lill, D. X. Cao, M. Schrock, J. Vollbrecht, J. Huang, T. Nguyen-Dang, V. V. Brus, B. Yurash, D. Leifert, G. C. Bazan, T. Q. Nguyen, *Adv. Mater.* **2020**, *32*, 1908120.

[28] Z. S. Parr, R. B. Rashid, B. D. Paulsen, B. Poggi, E. Tan, M. Freeley, M. Palma, I. Abrahams, J. Rivnay, C. B. Nielsen, *Adv. Electron. Mater.* **2020**, *6*, 2000215.

[29] D. Blasi, F. Viola, F. Modena, A. Luukkonen, E. MacChia, R. A. Picca, Z. Gounani, A. Tewari, R. Österbacka, M. Caironi, Z. M. Kovacs Vajna, G. Scamarcio, F. Torricelli, L. Torsi, *J. Mater. Chem. C* **2020**, *8*, 15312.

[30] J. Kawahara, P. A. Ersman, K. Katoh, M. Berggren, *IEEE Trans. Electron Devices* **2013**, *60*, 2052.

[31] P. Andersson Ersman, D. Nilsson, J. Kawahara, G. Gustafsson, M. Berggren, *Org. Electron.* **2013**, *14*, 1276.

[32] M. Afonso, J. Morgado, L. Alcácer, *J. Appl. Phys.* **2016**, *120*, 165502.

[33] M. Zabihipour, R. Lassnig, J. Strandberg, M. Berggren, S. Fabiano, I. Engquist, P. Andersson Ersman, *npj Flexible Electron.* **2020**, *4*, 15.

[34] Y. Yao, W. Huang, J. Chen, G. Wang, H. Chen, X. Zhuang, Y. Ying, J. Ping, T. J. Marks, A. Facchetti, *Proc. Natl. Acad. Sci. USA* **2021**, *118*, 2111790118.

[35] H. Sun, J. Gerasimov, M. Berggren, S. Fabiano, *J. Mater. Chem. C* **2018**, *6*, 11778.

[36] S. L. Bidinger, S. Han, G. G. Malliaras, T. Hasan, *Appl. Phys. Lett.* **2022**, *120*, 073302.

[37] D. Ohayon, G. Nikiforidis, A. Savva, A. Giugni, S. Wustoni, T. Palanisamy, X. Chen, I. P. Maria, E. Di Fabrizio, P. M. F. J. Costa, I. McCulloch, S. Inal, *Nat. Mater.* **2020**, *19*, 456.

[38] A. M. Pappa, D. Ohayon, A. Giovannitti, I. P. Maria, A. Savva, I. Uguz, J. Rivnay, I. McCulloch, R. M. Owens, S. Inal, *Sci. Adv.* **2018**, *4*, https://doi.org/10.1126/sciadv.aat0911.

[39] A. F. Paterson, A. Savva, S. Wustoni, L. Tsetseris, B. D. Paulsen, H. Faber, A. H. Emwas, X. Chen, G. Nikiforidis, T. C. Hidalgo, M. Moser, I. P. Maria, J. Rivnay, I. McCulloch, T. D. Anthopoulos, S. Inal, *Nat. Commun.* **2020**, *11*, 3004.

[40] A. Giovannitti, C. B. Nielsen, D.-T. Sbircea, S. Inal, M. Donahue, M. R. Niazi, D. A. Hanifi, A. Amassian, G. G. Malliaras, J. Rivnay, I. McCulloch, *Nat. Commun.* **2016**, *7*, 13066.

[41] C. G. Bischak, L. Q. Flagg, K. Yan, C. Z. Li, D. S. Ginger, *ACS Appl. Mater. Interfaces* **2019**, *11*, 28138.

[42] H. Sun, M. Vagin, S. Wang, X. Crispin, R. Forchheimer, M. Berggren, S. Fabiano, *Adv. Mater.* **2018**, *30*, 1704916.

[43] C. Y. Yang, D. Tu, T. P. Ruoko, J. Y. Gerasimov, H. Y. Wu, P. C. Harikesh, M. Massetti, M. A. Stoeckel, R. Kroon, C. Müller, M. Berggren, S. Fabiano, *Adv. Electron. Mater.* **2022**, *8*, 2100907.

[44] Y. Zhang, E. R. W. van Doremaele, G. Ye, T. Stevens, J. Song, R. C. Chiechi, Y. van de Burgt, *Adv. Mater.* **2022**, 2200393.

[45] F. A. Viola, B. Brigante, P. Colpani, G. Dell'Erba, V. Mattoli, D. Natali, M. Caironi, *Adv. Mater.* **2020**, *32*, 2002329.

[46] F. A. Viola, J. Barsotti, F. Melloni, G. Lanzani, Y.-H. Kim, V. Mattoli, M. Caironi, *Nat. Commun.* **2021**, *12*, 5842.

[47] P. Cosseddu, F. Viola, S. Lai, L. Raffo, L. Seminara, L. Pinna, M. Valle, R. Dahiya, A. Bonfiglio, in *SENSORS, 2014*, IEEE, Piscataway, NJ **2014**, pp. 1734–1736.

[48] E. Stucchi, A. D. Scaccabarozzi, F. A. Viola, M. Caironi, *J. Mater. Chem. C* **2020**, *8*, 15331.

[49] E. Stucchi, K. Maksimovic, L. Bertolacci, F. A. Viola, A. Athanassiou, M. Caironi, *J. Inf. Disp.* **2021**, *22*, 247.

[50] G. Mattana, A. Loi, M. Woytasik, M. Barbaro, V. Noël, B. Piro, *Adv. Mater. Technol.* **2017**, *2*, 1700063.

[51] T. Leydecker, Z. M. Wang, F. Torricelli, E. Orgiu, *Chem. Soc. Rev.* **2020**, *49*, 7627.

[52] A. Molazemhosseini, F. A. Viola, F. J. Berger, N. F. Zorn, J. Zaumseil, M. Caironi, *ACS Appl. Electron. Mater.* **2021**, *3*, 3106.

[53] Z. Chen, Y. Zheng, H. Yan, A. Facchetti, *J. Am. Chem. Soc.* **2009**, *131*, 8.

[54] D. Ohayon, A. Savva, W. Du, B. D. Paulsen, I. Uguz, R. S. Ashraf, J. Rivnay, I. McCulloch, S. Inal, *ACS Appl. Mater. Interfaces* **2021**, *13*, 4253.

[55] R. Kim, B. Kang, D. H. Sin, H. H. Choi, S.-K. Kwon, Y.-H. Kim, K. Cho, *Chem. Commun.* **2015**, *51*, 1524.

[56] R. Porrazzo, A. Luzio, S. Bellani, G. E. Bonacchini, Y. Y. Noh, Y. H. Kim, G. Lanzani, M. R. Antognazza, M. Caironi, *ACS Omega* **2017**, *2*, 1.

[57] C. M. Proctor, J. Rivnay, G. G. Malliaras, *J. Polym. Sci., Part B: Polym. Phys.* **2016**, *54*, 1433.

[58] Y. Khan, A. Thielens, S. Muin, J. Ting, C. Baumbauer, A. C. Arias, *Adv. Mater.* **2020**, *32*, 1905279.

[59] D. Heimfarth, M. Balcı Leinen, P. Klein, S. Allard, U. Scherf, J. Zaumseil, *ACS Appl. Mater. Interfaces* **2022**, *14*, 8209.

[60] F. Jakubka, S. B. Grimm, Y. Zakharko, F. Gannott, J. Zaumseil, *ACS Nano* **2014**, *8*, 8477.

[61] R. Matsidik, H. Komber, M. Sommer, *ACS Macro Lett.* **2015**, *4*, 1346.

[62] R. Matsidik, A. Luzio, S. Hameury, H. Komber, C. R. McNeill, M. Caironi, M. Sommer, *J. Mater. Chem. C* **2016**, *4*, 10371.